Copyright © 2011 by the Genetics Society of America
DOI: 10.1534/genetics.110.123505

Mapping the Epistatic Network Underlying Murine Reproductive Fatpad Variation

Joseph P. Jarvis*,†,[1] and James M. Cheverud*

**Department of Anatomy and Neurobiology, Washington University School of Medicine, St. Louis, Missouri, 63110 and †Department of Genetics, University of Pennsylvania, Philadelphia, Pennsylvania, 19104*

Manuscript received October 2, 2010
Accepted for publication November 3, 2010

ABSTRACT

Genome-wide mapping analyses are now commonplace in many species and several networks of interacting loci have been reported. However, relatively few details regarding epistatic interactions and their contribution to complex trait variation in multicellular organisms are available and the identification of positional candidate loci for epistatic QTL (epiQTL) is hampered, especially in mammals, by the limited genetic resolution inherent in most study designs. Here we further investigate the genetic architecture of reproductive fatpad weight in mice using the F_{10} generation of the LG,SM advanced intercross (AI) line. We apply multiple mapping techniques including a single-locus model, locus-specific composite interval mapping (CIM), and tests for multiple QTL per chromosome to the 12 chromosomes known to harbor single-locus QTL (slQTL) affecting obesity in this cross. We also perform a genome-wide scan for pairwise epistasis. Using this combination of approaches we detect 199 peaks spread over all 19 autosomes, which potentially contribute to trait variation including all eight original F_2 loci (*Adip1-8*), novel slQTL peaks on chromosomes 7 and 9, and several novel epistatic loci. Extensive epistasis is confirmed involving both slQTL confidence intervals (C.I.) as well as regions that show no significant additive or dominance effects. These results provide important new insights into mapping complex genetic architectures and the role of epistasis in complex trait variation.

THE development and elaboration of techniques such as interval mapping (Lander and Botstein 1989), composite interval mapping (CIM) (Zeng 1994), and methods based on complex pedigree structures (Jannink *et al.* 2001) have produced an extensive repertoire for the statistical exploration of genotype–phenotype relationships, especially for single loci. Using these approaches, genome-wide analyses have identified single-locus QTL (slQTL) underlying variance in characters as varied as agronomic traits and pest resistance in corn (Papst *et al.* 2004), life span in fruit flies (Wilson *et al.* 2006), alkylator-induced cancer susceptibility in mice (Fenske *et al.* 2006), murine skeletal morphology (Kenney-Hunt *et al.* 2008), and an ever-expanding list of human diseases and disorders including age-related macular degeneration (*e.g.*, Klein *et al.* 2005), type 2 diabetes (*e.g.*, Sladek *et al.* 2007; Zeggini *et al.* 2008), and Crohn's disase (*e.g.*, Duerr *et al.* 2006). In addition, several studies have successfully employed epistatic QTL (epiQTL) mapping strategies to describe multilocus networks (*e.g.*, Cheverud *et al.* 2001; Stylianou *et al.* 2006; Wentzell *et al.* 2007; Fawcett *et al.* 2008, 2010).

Supporting information is available online at http://www.genetics.org/cgi/content/full/genetics.110.123505/DC1 and the QTL archive at http://qtlarchive.org.

[1] *Corresponding author:* Tishkoff Lab, Department of Genetics, University of Pennsylvania, 422 Clinical Research Bldg., 415 Curie Blvd., Philadelphia, PA 19104-6145. E-mail: jarvisj@mail.med.upenn.edu

However, most mapping studies in model systems involve either F_2 intercross populations or recombinant inbred (RI) strain panels (see also Hanlon *et al.* 2006). These populations harbor limited recombination and so tend to identify relatively large confidence intervals, complicating the physiological investigation of statistical results. Furthermore, while RI strain sets represent a fourfold expansion of the F_2 recombination-based map, they require a minimum of 20 generations of brother–sister mating (Silver 1995) and the number of strains per set is usually low, especially in mammals. Conversely, the production of advanced intercross (AI) lines involves many generations of outbreeding in a relatively large population. This preserves heterozygosity, retains many more recombinant gametes in the gene pool, decreases the average size of segregating linkage blocks, and increases mapping resolution (Haldane and Waddington 1931; Bartlett and Haldane 1935; Hanson 1959a,b,c,d; Darvasi and Soller 1995; Rockman and Kruglyak 2008). Specifically, the F_{10} generation of a murine AI line represents an approximately fivefold expansion of the F_2 map and thus an improvement in resolution over both F_2 intercross and RI line study designs.

Obesity and related phenotypes are among the most intensively studied complex traits in mice and the LG,SM AI has proven particularly useful in the identification of adiposity QTL. Previous work in this cross has characterized over 70 loci contributing to variance in

fatpad weight, body weight, and relevant organ weights (Cheverud *et al.* 1999, 2001, 2004a,b; Fawcett *et al.* 2008). In addition, a recent study used the combined F_9 and F_{10} generations (Fawcett *et al.* 2010) to fine map loci for a suite of obesity-related characters and achieved an average confidence interval (C.I.) for fatpad loci of 4.14 Mb. These C.I.s were subsequently tested for epistasis and extensive interaction was confirmed, though several direct-effect loci identified in the F_2 and $F_{2/3}$ generations failed to replicate and were thus not included. However, in a full genome-wide scan for pairwise epistasis in the F_2 generation of this cross (Jarvis and Cheverud 2009) 38 fatpad loci, which were not identified using a single-locus mapping model, show significant epistatic interactions. Consistent with results from other experimental systems (reviewed in Phillips 2008) this suggests that many biologically relevant loci are invisible to single-locus scans. Thus, combining the increased genetic resolution of an F_{10} AI line study, with the full range of single-locus and epistatic mapping strategies promises to produce novel insights into the contribution of epistatic interactions to variation in reproductive fatpad weight in mice. Furthermore, the accumulating data on positional candidate genes (*e.g.*, Chehab 2008; Gat-Yablonski and Phillip 2008; Ichihara and Yamada 2008; Cheverud *et al.* 2010) provides the opportunity to explore functional hypotheses for identified loci and their interactions.

Utilizing the F_{10} generation of the LG,SM AI line (Cheverud *et al.* 2001), we further characterized the complex genetic architecture underlying murine reproductive fatpad weight. We first performed a slQTL scan on the original eight chromosomes harboring direct effect loci in the F_2 generation (1, 6–9, 12, 13, and 18) as well as the four shown to harbor slQTL in the combined F_9–F_{10} population (3, 4, 10, and 16) (Fawcett *et al.* 2010). Composite interval mapping and two QTL tests were subsequently performed, the latter when multiple loci on a single chromosome were suspected. Finally, we carried out a full genome-wide scan for pairwise epistasis. To identify the most meaningful set of loci to screen for candidate genes, marker genotypes representing slQTL and epiQTL that exceeded their appropriate thresholds were combined in linear models, first for each chromosome separately and ultimately the entire genetic system. Confidence intervals for peaks that remained significant in the full model were screened for positional candidate loci and potential physiological interactions via both the Mouse Genome Informatics (MGI) database (www.informatics.jax.org/) and a literature search.

MATERIALS AND METHODS

Data: The population analyzed is the F_{10} generation ($N = 1298$; 85 full-sib families; average litter size 8.45) of an AI line, generated from an F_2 intercross of the inbred mouse strains SM/J and LG/J (Chai 1956a,b; Cheverud *et al.* 1996, 2001; Kramer *et al.* 1998; Vaughn *et al.* 1999). The animal facility is maintained at a constant temperature of 21° with 12-hour light/dark cycles. Animals were fed a standard rodent chow (PicoLab Rodent Chow 20 (no. 5053) with 12% of its energy from fat, 23% from protein, and 65% from carbohydrate) *ad libitum* and were weaned at 3 weeks of age. After weaning, animals were housed in single-sex cages containing no more than five individuals.

Between the F_2 and F_{10} generations, the population was maintained at an effective size of ~300 with 75 mating pairs and no variance in family size. Mating between littermates was actively avoided. At greater than 13 weeks of age, animals were killed and necropsies performed. The reproductive fatpads of each animal were removed, combined, and weighed on a digital scale to the nearest 100th of a gram. Phenotypes were statistically corrected for age at necropsy, sex, litter size, and parity status (whether or not they were mated to produce the F_{11}), using multiple regression, and the residuals used for further analysis. Genotypes for each individual were obtained at 1470 polymorphic SNPs across the genome by GoldenGate Assay (Illumina; San Diego) using DNA extracted from liver tissue obtained at necropsy. Intermarker genotypes were imputed at 1-cM intervals using the equations of Haley and Knott (1992).

Mapping analyses: A single-locus QTL (slQTL) scan at all measured and imputed loci was first conducted on chromosomes 1, 3, 4, 6–10, 12, 13, 16, and 18 using the regression model

$$Y_i = \mu + a \times X_{ai} + d \times X_{di} + \text{error}, \quad (1)$$

where Y_i is the vector of corrected phenotypes, μ is a constant, and X_{ai} and X_{di} are the vectors of genotype scores; a and d are the fitted additive and dominance regression coefficients, respectively. The sums of squares for both model terms were pooled for significance testing. The results of the full genome-wide slQTL mapping in the combined F_9–F_{10} generations were previously reported (Fawcett *et al.* 2010).

CIM (Zeng 1994) was applied to the identified, preliminary confidence intervals using the following model:

$$Y_{ijk} = \mu + a \times X_{ai} + d \times X_{di} + \text{error} \,|\, X_{aj} X_{dj} X_{ak} X_{dk}. \quad (2)$$

In this case, X_{aj}, X_{dj}, X_{ak}, and X_{dk} represent vectors of genotype scores at loci >20 F_{10} cM up- and downstream of the confidence interval on whose effects the within-interval regressions were conditioned. This eliminates the effects of proximal and distal QTL on the same chromosome from being confounded with the target QTL. When multiple peaks on the same chromosome were suggested, the fit of all pairwise two-locus models were compared to the appropriate single-locus case using a χ^2 test with 2 degrees of freedom (d.f.) ($\chi^2_{\text{crit}} = 2 * \text{abs}[\ln(1/p_{\text{one}}) - \ln(1/p_{\text{two}})]$, where p_{one} and p_{two} are *P*-values from the one- and two-locus models, respectively (Sokal and Rohlf 1995).

Finally all genome-wide, between-chromosome, pairwise combinations of measured and imputed autosomal loci were tested using the following epistatic mapping model:

$$\begin{aligned} Y_{ij} = \mu &+ aa(X_{ai} \times X_{aj}) + ad(X_{ai} \times X_{dj}) + da(X_{di} \times X_{aj}) \\ &+ dd(X_{di} \times X_{dj}) + \text{error} \,|\, X_{ai} X_{di} X_{aj} X_{dj}, \end{aligned} \quad (3)$$

where *aa*, *ad*, *da*, and *dd* are the additive-by-additive, additive-by-dominance, dominance-by-additive, and dominance-by-dominance epistasis regression coefficients, and X_{ai} X_{di} X_{aj} X_{dj} represent vectors of the corresponding additive and dominance genotypes at the two loci involved. The sums of squares and degrees of freedom for all four epistatic compo-

nents were pooled for initial significance testing. The raw probability associated with each multiple regression for all mapping analyses above was transformed to a linear scale using the base 10 logarithm of the inverse of the probability of no epistasis ($LPR = \log_{10}(1/p)$), producing values comparable to LOD scores obtained through maximum likelihood analysis (Lander and Botstein 1989).

Thresholds: Interpretation of these analyses is complicated both by the large number of comparisons involved as well as the family structure present in the population. To account for these two issues simultaneously, simulations were performed using the known pedigree of all individuals between the F_2 and F_{10} generations to generate a null distribution of expected effects from which the appropriate single-locus LPR threshold was determined (Fawcett *et al.* 2008, Norgard *et al.* 2009). Given a heritability of reproductive fatpad weight in the F_{10} of 0.47 (from sib correlations) chromosome-specific thresholds for identifying novel slQTL ranged from 6.15 (chromosome 8) to 6.6 (chromosome 1). The experiment-wide threshold for novel slQTL detection was 7.34. For the purposes of replication, a corrected pointwise threshold (equivalent to $P = 0.05$) of 3.32 was applied for slQTL peaks within previously identified confidence intervals.

Following the method described in Fawcett *et al.* (2010), the analysis-wide epistasis threshold for the identification of novel interactions was calculated to be 8.33. The threshold for tests between a given slQTL and all other unlinked markers in the analysis was 6.06 and the analogous chromosome-specific thresholds ranged from 4.73 (chromosome 8) to 5.25 (chromosome 1). The corrected pointwise threshold for epistatic tests between two slQTL was 3.44. Tests involving slQTL are partially protected from multiple comparisons as they were identified with independent information.

Confidence intervals: Due to the complexity of our mapping strategy, the conventional 1 LPR drop criterion was applied to define all reported confidence intervals. When multiple peaks, either slQTL, epiQTL, or both occurred in the same region, the most proximal and most distal 1 LPR drop was used to determine C.I. endpoints. C.I.s for slQTL peaks were also calculated for each location individually using the standard deviation of the simulated distribution of 1000 mapping iterations involving known effects on simulated chromosomes (Norgard *et al.* 2009). The two techniques yielded very similar C.I. for all slQTL, although the simulation-based intervals were slightly smaller.

Linear models: We constructed and evaluated separate chromosome-specific models using the linear model function in R (R Development Core Team 2009) before combining their results into a full model of the genetic system. This process began with terms representing each significant effect at all slQTL peaks identified by the single-locus model (Equation 1) and composite interval mapping (Equation 2). For example, the chromosome 1 model (see Figure 1A) began with five slQTL terms representing the additive ($P = 0.00726$) and dominance ($P = 0.0007$) effects at 20.15 Mb, the additive ($P = 0.000268$) and dominance ($P = 0.0383$) effects at 70.77 Mb and the dominance effect ($P = 1.06 \times 10^{-06}$) at 134.82 Mb. The additive effect at 134.82 Mb was nonsignificant in the slQTL mapping model ($P = 0.868$) and so was not included. Likewise, the chromosome 13 model (see Figure 1B) included two terms representing the additive effects at 53.54 Mb ($P = 3.05 \times 10^{-06}$) and 90.61 Mb ($P = 4.88 \times 10^{-05}$), respectively. In this case, neither dominance effect was significant in the slQTL mapping model ($P = 0.798$ and $P = 0.634$) and so both were excluded. When considered jointly, some individual terms (*e.g.*, the dominance effect only at 70.77 Mb on chromosome 1) no longer remained significant ($P < 0.05$) in type I ANOVA tables (using the "anova" function). Such terms were removed. For those chromosomes not found to harbor slQTL, a similar process was performed beginning with all significant interactions.

Next, individual coefficients from the epistatic mapping model (*aa, ad, da, dd*; Equation 3) at all peaks that exceeded their appropriate thresholds in the epiQTL scan were similarly examined to determine the type or types of interactions occurring. Terms representing all significant interactions were then added stepwise to each appropriate chromosome-specific model. Only epistatic terms that remained significant ($P < 0.05$) in both type I and type II ANOVA tables, using the R functions "anova" and "Anova" (the latter from the package "car"), respectively, and did not cause any established additive or dominance effects to become nonsignificant ($P < 0.05$) were retained to define each final chromosome-specific model. These stringent criteria were established to obtain a tractable number of high-confidence C.I. to screen for positional candidates and physiological interactions.

Next, additive and dominance terms from all chromosome-specific models were combined and terms that became nonsignificant in either type I or type II ANOVA tables (or both) were culled to define the "slQTL system." This model included 20 terms at 18 loci (15 additive and 5 dominance; boldface type in supporting information, Table S1). Epistasis terms significant in the chromosome-specific models were then added stepwise to the slQTL system as above to define the "full model." In addition to the 20 marginal-effect terms, this model includes 23 interactions involving 26 different epiQTL confidence intervals. Finally, since many epiQTL peaks occur at locations not represented in the slQTL system, the appropriate additive and dominance terms for each interaction were added to the full model to ensure that the identified epistatic contributions were not unduly biased upward by variance attributable to single-locus effects. This had relatively little effect and resulted in the elimination of only 3 interactions, all of which are significant in type I tests. The results from the full model are reported with these nominally significant terms noted in boldface type (Table 1, see below).

Candidate genes: All C.I.s for peaks identified in the full model were screened for plausible positional candidate genes and known interactions. This involved both queries of the MGI database for functional variants affecting adiposity as well as a broad literature search and was intended to generate meaningful and testable physiological hypotheses regarding the observed statistical associations.

RESULTS

Replication and identification: Significant marginal effects, epistatic effects, or both are observed in the F_{10} population on all eight chromosomes harboring the original *Adip* loci and three of the four additional chromosomes implicated in the combined F_9–F_{10} slQTL scan (Figure S1). In the F_{10} alone, there were no significant slQTL on chromosome 16. Similar to the results of Fawcett *et al.* (2010), peak LPR scores from either the single-locus scan or composite interval mapping at or near the confidence intervals of five *Adip* loci exceeded the experiment-wide threshold (7.34) for novel QTL detection (*Adip1*, LPR = 9.2; *Adip2*, LPR = 8.9; *Adip3*, LPR = 8.3; *Adip5*, LPR = 9.6; and *Adip8*, LPR = 12.3). All three remaining F_2 loci exceed the pointwise threshold (3.32) required for tests within previously defined confidence intervals (*Adip4*, LPR =

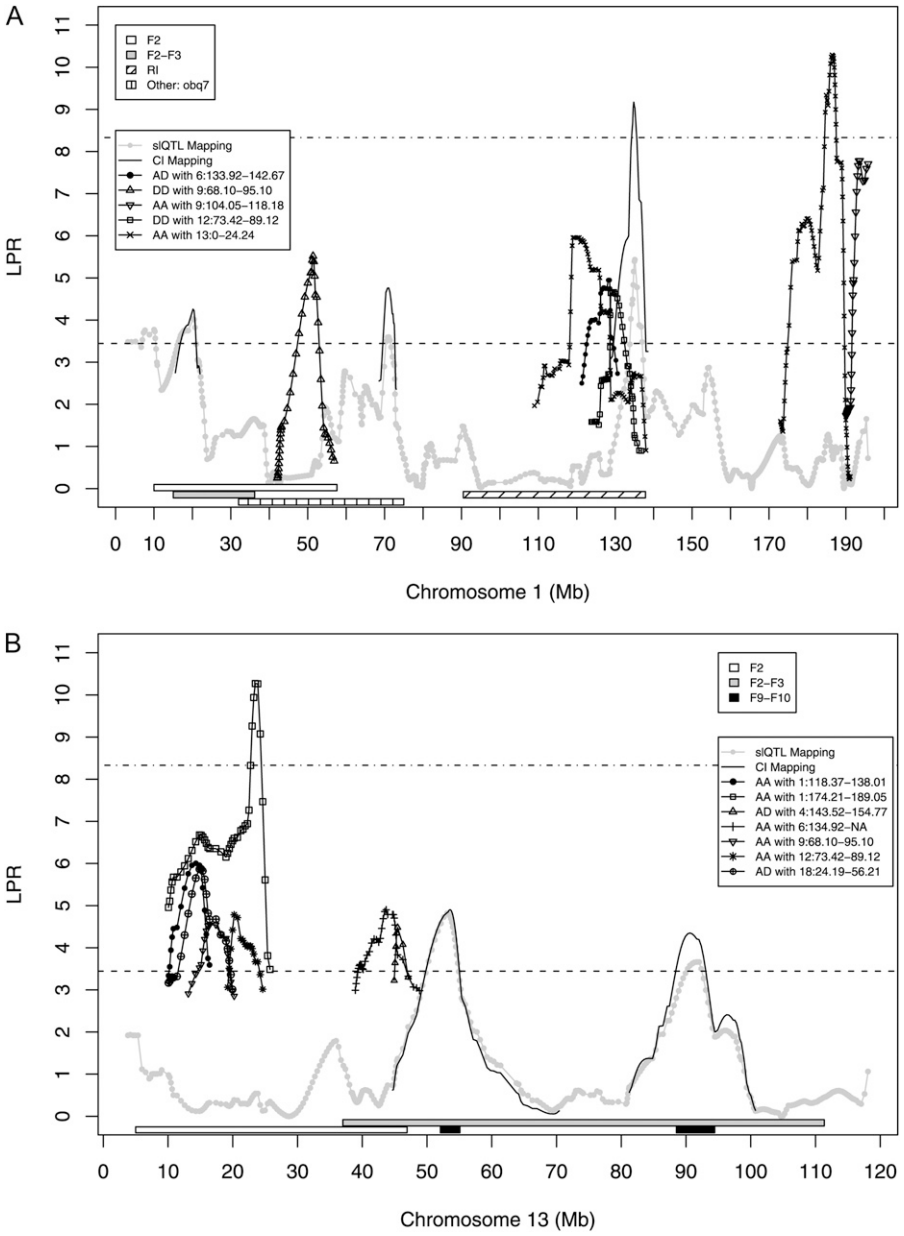

Figure 1.—Mapping results of significant terms from the full model of reproductive fatpad weight in the LG,SM AI line for chromosomes 1 (A) and 13 (B). Results from the single-locus model are given as connected shaded dots, composite interval mapping as smooth solid lines, and epistatic interactions by other connected shapes. Confidence intervals from previous analyses are represented by horizontal bars below the QTL plot.

5.6; *Adip6*, LPR = 5.24; and *Adip7*, LPR = 4.8). Additional slQTL on chromosomes 3, 4, and 10 also replicated. Interestingly, the chromosome 4 locus (*Adip24*) (Fawcett *et al.* 2010; LPR = 12.65) roughly corresponds to two loci previously reported in the literature as *Adip11* and *Adip12* in a cross between C57BL/6J and DBA/2J (Keightley *et al.* 1996; Brockmann *et al.* 1998; Stylianou *et al.* 2006). Finally, composite interval mapping revealed novel loci on chromosomes 7 and 9 that both exceed their appropriate chromosome-specific thresholds of 6.36 and 6.38, respectively. A total of 22 potential marginal effect peaks were identified (Table S1).

epiQTL mapping: In the genome-wide scan for epistasis, 177 peaks involving 217 interactions exceeded their appropriate significance thresholds and physically cluster into ~51 potential epiQTL (Table S1). Additive-by-additive interactions were the most common (98), additive-by-dominance or dominance-by-additive were the next most common (97), and dominance-by-dominance interactions were the most rare (22). Consistent with the results of Jarvis and Cheverud (2009) and several other studies (see Phillips 2008), many of these occurred at locations showing no significant marginal effects in this cross, though some occurred at locations significant in slQTL scans in other crosses (Table 1; Figure 1; Table S1; Figure S2; Figure S3; Figure S4; Figure S5; Figure S6; Figure S7; Figure S8; Figure S9; Figure S10; Figure S11; Figure S12; Figure S13; Figure S14; Figure S15; Figure S16; Figure S17; Figure S18; Figure S19; Figure S20).

Linear models: In total, we identified 199 slQTL and epiQTL peaks that potentially contribute to trait variation. These cluster into roughly 73 confidence intervals

TABLE 1

Results from the full linear model of the epistatic network underlying murine reproductive fatpad weight in the LG,SM AI line

Chr 1	C.I. 1 begin (Mb)	C.I. 1 end (Mb)	Peak 1 (Mb)	Chr 2	C.I. 2 begin (Mb)	C.I. 2 end (Mb)	Peak 2 (Mb)	slQTL LPR	Peak SNP 1	Peak SNP 2	Epistatic LPR	Effect(s)	Threshold type	Threshold	Reported Adipose QTL in CI(s)	QTL reference(s)	Candidates (C.I. 1)	Candidates (C.I. 2)
1	16.40	21.28	20.15	NA	NA	NA	NA	4.26	rs6334092	NA	NA	A,D	Pointwise	3.32	Adip1; Obq2	Cheverud *et al.* 2001; Fawcett *et al.* 2008; Taylor and Phillips 1996	Pkhd1	NA
1	65.79	74.08	70.77	NA	NA	NA	NA	4.76	rs6323094	NA	NA	A	Pointwise	6.60	Obq7	Taylor *et al.* 2001	Vwc2l; Fn1	NA
1	118.37	138.01	134.82	NA	NA	NA	NA	9.17	gnf01.132.831	NA	NA	A	Pointwise	3.32	Obsty1; Gwth1; Obq17	Cheverud *et al.* 2004; Yi *et al.* 2006; Ishimori *et al.* 2004	Pik3c2b	NA
3	20.54	27.82	22.51	NA	NA	NA	NA	5.56	rs13477017	NA	NA	A	Pointwise	3.32	None	None	Nlgn1; Ghsr	NA
4	9.71	11.92	10.83	NA	NA	NA	NA	4.78	rs13477558	NA	NA	D	Pointwise	3.32	Unnamed RI QTL	Cheverud *et al.* 2004	Plekhf2	NA
4	78.28	90.30	79.46	NA	NA	NA	NA	11.87	CEL-4-78089985	NA	NA	A	Pointwise	3.32	Adip11; Adip24; Adip11a	Fawcett *et al.* 2008; Fawcett *et al.* 2010; Stylianou *et al.* 2006	Tyrp1	NA
6	114.73	121.97	117.73	NA	NA	NA	NA	5.01	mCV23042866	NA	NA	D	Pointwise	3.32	Adip2; Igf1sl1	Cheverud *et al.* 2001; Rosen *et al.* 2005	Adipor2; Ankrd26; Pparg	NA
6	133.92	142.67	134.20	NA	NA	NA	NA	8.89	rs13479053	NA	NA	A	Pointwise	3.32	Adip2	Cheverud *et al.* 2001	Lrp6; Grin2b; Cdkn1b	NA
7	30.18	44.44	37.21	NA	NA	NA	NA	4.08	rs6217275	NA	NA	D	Pointwise	3.32	Adip3; Adip3A; Adip3Ab	Cheverud *et al.* 2001; Fawcett *et al.* 2008; Fawcett *et al.* 2010	Tshz3; Plekhf1	NA
7	59.83	77.73	63.51	NA	NA	NA	NA	6.85	rs3717293	NA	NA	A,D	Pointwise	3.32	Tabw; Adip3Ad; Adip25; Obq1	Kim *et al.* 2001; Fawcett *et al.* 2010; Taylor and Phillips 1996	Nipa1; Nipa2; Gabrg3; Gabra5; Gabrb3	NA
7	132.03	143.20	135.24	NA	NA	NA	NA	6.38	CEL-7-116160192	NA	NA	A	New slQTL chr7	6.36	Bsbob2	Yi *et al.* 2004	Trim72	NA

(*continued*)

TABLE 1

(Continued)

Chr 1	C.I. 1 begin (Mb)	C.I. 1 end (Mb)	Peak 1 (Mb)	Chr 2	C.I. 2 begin (Mb)	C.I. 2 end (Mb)	Peak 2 (Mb)	slQTL LPR	Peak SNP 1	Peak SNP 2	Epistatic LPR	Effect(s)	Threshold type	Threshold	Reported Adipose QTL in CI(s)	QTL reference(s)	Candidates (C.I. 1)	Candidates (C.I. 2)
8	64.98	90.95	84.79	NA	NA	NA	NA	4.76	rs13479860	NA	NA	A	Pointwise	3.32	Adip4	Cheverud *et al.* 2001; Fawcett *et al.* 2008	Il15	NA
9	61.70	67.72	65.39	NA	NA	NA	NA	6.98	rs13480247	NA	NA	A	New slQTL chr9	6.38	None	None	Mtfmt	NA
9	118.30	125.00	118.88	NA	NA	NA	NA	9.64	rs6316481	NA	NA	A	Pointwise	3.32	Adip5; Adip5a; Adip5b; Adip5c; Obq18	Cheverud *et al.* 2001; Fawcett *et al.* 2008; Fawcett *et al.* 2010; Ishimori *et al.* 2004	Acvr2b	NA
12	60.62	67.43	64.06	NA	NA	NA	NA	5.24	mCV24690992	NA	NA	A	Pointwise	3.32	Adip6; Adip16; Fob2	Fawcett *et al.* 2008; Stylianou *et al.* 2006; Horvat *et al.* 2000	Lrfn5	NA
13	40.74	55.35	53.54	NA	NA	NA	NA	4.90	rs3699522	NA	NA	A	Pointwise	3.32	Adip7; Adip18; Adip18a; Pfat3	Cheverud *et al.* 2001; Fawcett *et al.* 2008; Fawcett *et al.* 2010; Keightley *et al.* 1998	Cplx2; Drd1a	NA
18	24.19	56.21	48.82	NA	NA	NA	NA	4.83	rs3684561	NA	NA	A	Pointwise	3.32	Adip8; Adip8a; Adip8b; Kcal1; Mnif2	Cheverud *et al.* 2001; Fawcett *et al.* 2010; Smith Richards *et al.* 2002	Sema6a; Hsd17b4	NA
18	58.77	80.76	63.84	NA	NA	NA	NA	12.31	rs13483398	NA	NA	A	Pointwise	3.32	Adip8; Adip8c; Adip8d; Obsty4	Cheverud *et al.* 2001; Fawcett *et al.* 2008; Fawcett *et al.* 2010; Cheverud *et al.* 2004	Adrb2; Htr4	NA

(*continued*)

TABLE 1

(Continued)

Chr 1	C.I. 1 begin (Mb)	C.I. 1 end (Mb)	Peak 1 (Mb)	Chr 2	C.I. 2 begin (Mb)	C.I. 2 end (Mb)	Peak 2 (Mb)	slQTL LPR	Peak SNP 1	Peak SNP 2	Epistatic LPR	Effect(s)	Threshold type	Threshold	Reported Adipose QTL in CI(s)	QTL reference(s)	Candidates (C.I. 1)	Candidates (C.I. 2)
1	42.41	52.71	51.38	9	68.10	95.10	77.25	NA	rs13475863	rs13480288	5.52	DD	QTL × QTL epi	3.44	Adip1; Obq7; Adip5; Mob8	Cheverud *et al.* 2001; Taylor *et al.* 2001; Mehrabian *et al.* 1998	Gls	Gclc
1	118.37	138.01	128.52	6	133.92	142.67	141.48	NA	rs6228473	rs8268650	4.95	AD	QTL × QTL epi	3.44	Obsty1; Gwth1; Obq17; Adip2	Cheverud *et al.* 2001; Cheverud *et al.* 2004; Yi *et al.* 2006; Ishimori *et al.* 2004	Gpr39	Pde3a
1	118.37	138.01	128.84	12	73.42	89.12	75.11	NA	rs13476100	rs3687032	4.64	DD	QTL × QTL epi	3.44	Obsty1; Gwth1; Obq17; Adip6	Cheverud *et al.* 2001; Cheverud *et al.* 2004; Yi *et al.* 2006; Ishimori *et al.* 2004	Gpr39	Hif1a
1	174.21	189.05	186.63	13	0.00	24.24	23.48	NA	mCV24555989	gnf13.020.621	10.27	AA	QTL × chr1 epi	5.25	Obq9	Taylor *et al.* 2001	Hlx	Abt1
4	**30.53**	**39.16**	**36.58**	**9**	**118.30**	**125.00**	**123.70**	**NA**	**rs13477649**	**rs8241505**	**6.03**	**DD**	**QTL × QTL epi**	**3.44**	**Unnamed RI QTL; Dob2; Obq18**	Cheverud *et al.* 2004; Ishimori *et al.* 2004; West *et al.* 1994	**Cga**	**Slc6a20a; Slc6a20b**
4	125.68	139.92	130.91	7	132.03	143.20	139.70	NA	rs3673061	rs8236684	4.93	AD	QTL × QTL epi	3.44	Adip12; Qbis1; Afpq2; Adip3	Cheverud *et al.* 2001; Stylianou *et al.* 2006; Togawa *et al.* 2006; Brockmann *et al.* 2000	Ptpru	Oat
4	143.52	154.77	152.94	7	132.03	143.20	141.88	NA	rs6378384	rs3719258	4.69	AD	QTL × QTL epi	3.44	Adip12; Adip3	Cheverud *et al.* 2001; Stylianou *et al.* 2006	Ajap1	Adam12
6	**33.46**	**46.84**	**37.64**	**9**	**118.30**	**125.00**	**123.70**	**NA**	**rs13478717**	**rs8241505**	**5.11**	**DA**	**QTL × chr6 epi**	**5.09**	**Dob2; Obq18**	Ishimori *et al.* 2004; West *et al.* 1994	**Trim24**	**Ccr9**

(*continued*)

TABLE 1

(Continued)

Chr 1	C.I. 1 begin (Mb)	C.I. 1 end (Mb)	Peak 1 (Mb)	Chr 2	C.I. 2 begin (Mb)	C.I. 2 end (Mb)	Peak 2 (Mb)	slQTL LPR	Peak SNP 1	Peak SNP 2	Epistatic LPR	Effect(s)	Threshold type	Threshold	Reported Adipose QTL in CI(s)	QTL reference(s)	Candidates (C.I. 1)	Candidates (C.I. 2)
6	53.92	71.82	54.18	7	102.32	108.47	105.10	NA	rs13478762	UT-7-90.803899	5.13	AA	QTL × chr7 epi	4.96	Adip2; Obq13	Cheverud *et al.* 2001; Taylor *et al.* 2001	Crhr2; Ghrhr	Capn5
7	132.03	143.20	137.17	8	42.26	57.10	50.65	NA	rs8236684	rs13479769	5.08	AA	QTL × chr8 epi	4.73	Bsbob2	Yi *et al.* 2004	Fgfr2	Ing2
8	124.83	129.12	127.97	9	20.24	39.76	23.57	NA	rs6300613	rs13480112	5.57	AD	QTL × chr9 epi	4.99	Obsty2	Cheverud *et al.* 2004	Disc1	Npsr1
9	20.24	39.76	31.31	12	108.99	120.28	111.04	NA	CEL-9-29909656	CEL-12-104545022	5.36	AA,DD	QTL × chr9 epi	4.99	Carfhg2	Corva *et al.* 2001	Kcnj5	Dlk1; Meg3; Rtl1
9	104.05	118.18	109.62	1	191.98	NA	193.61	NA	rs3723953	rs13476308	7.78	AA	QTL × chr1 epi	5.99	Adip5;Dob2	Cheverud *et al.* 2001; West *et al.* 1994	Fbxw cluster	Nek2
12	108.99	120.28	113.11	1	191.98	NA	195.79	NA	rs13481651	rs13476312	6.06	DA	QTL × chr1 epi	5.25	Adip6; Bsbob4; Mob3	Cheverud *et al.* 2001; Fawcett *et al.* 2008; Yi *et al.* 2004; Warden *et al.* 1995	Traf3	Hsd11b1
13	0.00	24.24	14.85	1	118.37	138.01	119.02	NA	rs13481702	rs3694226	5.96	AA	QTL × chr1 epi	5.25	Adip7	Cheverud *et al.* 2001	Inhba	Inhbb
13	0.00	24.24	17.38	9	68.10	95.10	82.84	NA	rs3678616	rs13480312	4.54	AA	QTL × QTL epi	3.44	Adip7; Adip5	Cheverud *et al.* 2001	Inhba	Htr1b
13	0.00	24.24	20.21	12	73.42	89.12	82.08	NA	rs6314295	rs3654718	4.78	AA	QTL × QTL epi	3.44	Adip7; Adip6	Cheverud *et al.* 2001	Olfactory receptor cluster	Slc8a3
13	40.74	55.35	43.69	6	80.99	92.88	89.62	NA	rs13481789	rs13479099	4.90	AA	QTL × QTL epi	3.44	Adip7; Adip18; Adip18a; Pfat3; Adip2	Cheverud *et al.* 2001; Fawcett *et al.* 2008; Fawcett *et al.* 2010; Keightley *et al.* 1998	Ranbp9	Alms1

(*continued*)

TABLE 1

(Continued)

Chr 1	C.I. 1 begin (Mb)	C.I. 1 end (Mb)	Peak 1 (Mb)	Chr 2	C.I. 2 begin (Mb)	C.I. 2 end (Mb)	Peak 2 (Mb)	slQTL LPR	Peak SNP 1	Peak SNP 2	Epistatic LPR	Effect(s)	Threshold type	Threshold	Reported Adipose QTL in CI(s)	QTL reference(s)	Candidates (C.I. 1)	Candidates (C.I. 2)
13	40.74	55.35	45.45	4	143.52	154.77	152.94	NA	rs3688207	rs6378384	4.48	AD	QTL × QTL epi	3.44	Adip7; Adip18; Adip18a; Pfat3; Adip12	Cheverud *et al.* 2001; Fawcett *et al.* 2008; Fawcett *et al.* 2010; Stylianou *et al.* 2006; Keightley *et al.* 1998	Atxn1	Kcnab2
18	24.19	56.21	37.51	12	60.62	67.43	64.06	NA	gnf18.033.953	mCV24690992	5.88	AD	QTL × QTL epi	3.44	Adip8; Adip8a; Adip8b; Kcal1; Mnif2; Adip6	Cheverud *et al.* 2001; Fawcett *et al.* 2010; Smith Richards *et al.* 2002	Pcdhb cluster	Lrfn5
18	**24.19**	**56.21**	**37.93**	**13**	**0.00**	**24.24**	**15.11**	**NA**	**gnf18.033.953**	**rs13481702**	**5.87**	**DA**	**QTL × QTL epi**	**3.44**	**Adip8; Adip8a; Adip8b; Kcal1; Mnif2; Adip7**	Cheverud *et al.* 2001; Fawcett *et al.* 2010; Smith Richards *et al.* 2002	**Pcdhb cluster**	**Gli3**
18	24.19	56.21	50.47	7	30.18	44.44	30.56	NA	rs13483356	rs13479174	5.76	AD	QTL × QTL epi	3.44	Adip8; Adip8a; Adip8b; Kcal1; Mnif2; Adip3	Cheverud *et al.* 2001; Fawcett *et al.* 2010; Smith Richards *et al.* 2002	Hsd17b4	Lrfn3

Chromosome, confidence intervals (Mb), peak locations (Mb), peak LPR scores, nearest SNP to the peak, effect-type threshold, and threshold value are all given for each term. The appropriate references for any *a priori* hypotheses are listed along with positional candidate loci for both slQTL and epiQTL. Terms in boldface type are nominally significant ($P > 0.05$) when additive and dominance effects for all interactions are included in the model.

showing a variety of combinations of additive, dominance, and epistatic effects (Table S1). To identify the most robust signals, we systematically added vectors of genotype scores representing each into linear models and determined the set that is simultaneously significant in both type I and type II tests. We began by establishing a single-locus model that contained all slQTL peaks that remain significant together. This slQTL system includes 20 marginal-effect terms (15 additive and 5 dominance) and shows an adjusted R^2 value of 0.2254 (F statistic = 18.64 on 20 and 1281 d.f.). We next added epistatic peaks stepwise to generate a full model of the genetic system. This full model (Table 1) includes 23 additional interaction terms (9 *aa*, 10 *ad/da*, and 4 *dd*) involving 26 different epiQTL confidence intervals and shows an adjusted R^2 value of 0.3322 (F statistic = 15.71 on 43 and 1257 d.f.). Using a χ^2 goodness-of-fit test with 23 (43–20) d.f. this represents a highly significant improvement in fit over the base slQTL model ($P < 10^{-25}$). Following the addition of all marginal terms involved in epistasis, three interaction terms become nonsignificant at the $P < 0.05$ level in either type I or type II tables or both (boldface terms in Table 1). Removing these interactions from the full model, its adjusted R^2 value is 0.3220 (F statistic = 16.07 on 40 and 1260 d.f.), which also represents a highly significant improvement in model fit ($P < 10^{-20}$).

Positional candidates: While in-depth functional assays and other detailed molecular studies are required to sort out the biological basis of QTL and their interactions, examination of positional candidate genes in slQTL confidence intervals suggests testable physiological hypotheses for several observed statistical effects. In general, confidence intervals contain a variety of candidate loci including transcription factors, components of various signaling cascades (*e.g.*, the *Wnt*, *Insulin*, and *Igf* signaling networks), neuroendocrine hormones and their receptors, as well as genes directly implicated in glucose processing and metabolism. For example, the C.I. found at 6:133.92–142.67 Mb contains the promising candidate *Lrp6*, a low-density lipoprotein receptor-related protein that is thought to contribute to variation in a variety of metabolic risk factors in humans (Kahn *et al.* 2007; Mani *et al.* 2007) and *Cdkn1b*, a cyclin-dependent kinase inhibitor with known effects on pancreatic islet mass in diabetic mice (Uchida *et al.* 2005). Both *Lrp6* and *Cdkn1b* have differences in expression level in white fat ($P = 3.82 \times 10^{-12}$ and 0.013, respectively) and in the liver ($P = 1.62 \times 10^{-13}$ and 7.48×10^{-8}, respectively) between the two parental lines in this cross (J. M. Cheverud, unpublished results). The C.I. 18:58.77–80.76 Mb shows potential functional links to mammalian neurotransmitter signaling via *Htr4* (Gardner *et al.* 2008), as do 13:40.74–55.35 Mb via *Cplx2* (Brachya *et al.* 2006) and *Drd1a* (de Leeuw van Weenen *et al.* 2009). In addition, the region 6:114.73–121.97 Mb contains neuroendocrine candidates *Adipor2* (Yamauchi *et al.* 2007; Ziemke and Mantzoros 2010) and *Ankrd26* (Bera *et al.* 2008), which also shows a significant difference in expression in liver between LG/J and SM/J ($P = 0.0002$) (J. M. Cheverud, unpublished results). Together, these loci suggest a functionally similar genetic architecture to the emerging picture of type 2 diabetes in humans (Doria *et al.* 2008).

There are also a number of strong candidate loci for observed epistatic interactions. The most striking involves the C.I.s 13:0–24.24 Mb and 1:118.37–138.01 Mb, which contain *Inhba* and *Inhbb*, respectively. The proteins encoded by these loci are components of the Activin and Inhibin complexes, which have wide-ranging effects on a variety of physiologic, homeostatic, and metabolic processes including mammalian reproduction, inflammation, and adipocyte differentiation (Woodruff and Mather 1995; Hirai *et al.* 2005; Werner and Alzheimer 2006). Interestingly, 13:0–24.24 Mb participates in five separate interactions that are significant in the full model (Table 1) and appears to interact with a region (9:68.10–95.10 Mb) containing an important receptor for serotonin (*Htr1b*).

Glutamate signaling and metabolism are also likely to underlie a portion of fatpad variation due to epistasis in this cross. The interacting epiQTL CI 1:42.41–52.71 Mb and 9:68.10–95.10 Mb contain the enzyme that catalyses the first reaction in the primary pathway for the renal catabolism of glutamine (*Gls*) and the first rate-limiting enzyme in glutathione synthesis (*Gclc*), respectively. *Gls* also shows differential expression in white fat cells between the parental lines ($P = 0.00097$). Ghrelin and its associated pathways also appear as likely candidates. For example, 1:118.37–138.01 Mb contains *Gpr39*, a member of the ghrelin receptor family. This C.I. interacts with 6:133.92–142.67 Mb, which harbors *Pde3a*, a locus known to be downstream of ghrelin signaling in platelets (Elbatarny *et al.* 2007) and which shows significant differences in gene expression in white fat between SM/J and LG/J ($P = 0.00018$) and 12:73.42–89.12 Mb, which contains *Hif1a*, whose protein product increases the expression of *Vegf* (Hoffmann *et al.* 2008). Interestingly, *Vegfc* shows a significant difference in expression in white fat between the parental lines ($P = 0.001$) and Vegfb shows differences in liver ($P = 0.009$). Ghrelin is also known to increase the expression of *Vegf* in human luteal cells (Tropea *et al.* 2007) and *Vegf*, in turn, is thought to be an important regulator of adipogenesis and obesity (Cao 2007). A final interesting epiQTL CI is 12:108.99–120.28 Mb. It contains *Dlk1*, *Meg3*, and *Rtl1*, all three of which appear to participate in an interacting (and imprinted) network affecting growth in mice (Gabory *et al.* 2009).

DISCUSSION

While the family structure of an outbred population complicates some aspects of the mapping process, the F_{10}

(and later) generations of advanced intercross lines hold an intrinsic advantage in mapping resolution over more conventional study designs. Here this advantage translated into a variety of results with important implications for mapping complex trait variation and new insights into the genetic architecture of murine fatpad weight.

The first and most striking result of this analysis from a mapping perspective is the relatively low level of overlap in the physical positions of slQTL and epiQTL peaks despite the analytical bias toward finding epistasis involving slQTL due to their protected status with respect to multiple comparisons. Though slight discrepancies may be expected due to subtle patterns of linkage, larger map distances between peaks likely indicate that multiple functional variants are present. Indeed, when both types are observed in close proximity, epistatic peaks tend not to line up well with their single-locus counterparts and epiQTL are frequently observed in regions showing no significant marginal effects at all (Figure 1; Table 1; Table S1; Figure S1; Figure S2; Figure S3; Figure S4; Figure S5; Figure S6; Figure S7; Figure S8; Figure S9; Figure S10; Figure S11; Figure S12; Figure S13; Figure S14; Figure S15; Figure S16; Figure S17; Figure S18; Figure S19; Figure S20). This supports the notion that a relatively large number of variable, functionally relevant loci exert their influence on complex trait variation primarily via epistatic interactions rather than through conventional additive and dominance effects. It is also interesting to note that some regions interact with multiple locations in the genome. For example, proximal chromosome 13 (13:0–24.24 Mb) shows five significant interactions in the full model, including two with separate locations on chromosome 1. Identifying such repeated signals may be useful in developing significance thresholds that help ameliorate the penalties incurred by performing multiple comparisons. Such consistency may also help distinguish epiQTL at the center *vs.* the edges of functional networks.

Next, in keeping with observations in congenic lines (*e.g.*, Christians *et al.* 2006) as well as other recent slQTL mapping studies (Fawcett *et al.* 2010), F_2 confidence intervals were frequently observed to divide into multiple significant slQTL (Figure 1; Figure S1). Interestingly, we observe similar splitting of single-locus and epistatic signals. For example, at the proximal end of chromosome 1 (Figure 1A) marginal-effect peaks observed in the F_2, combined $F_{2–3}$, and in an intercross between SM and NZO (*obq7*; Taylor *et al.* 2001) appear to resolve in our mapping population into three distinct peaks with two marginal effect loci flanking an epiQTL. This suggests that the original F_2 and the subsequent $F_{2–3}$ signals in this cross were composites of both single-locus and epistatic effects and that the boundaries of previously reported C.I. may have been influenced by epistatic contributions to single-locus values. Thus, current estimates of the number of loci underlying trait variation are likely to be overly conservative and reported effect-size estimates are potentially biased by the presence of multiple, closely linked functional elements. Interestingly, it also suggests that confidence intervals identified in other intercross experiments, especially those that share a parental strain, can be productively evaluated under *a priori* epistatic hypotheses, which may also ease issues related to multiple testing. On this account, it is also striking that the epistatic network identified in Stylianou *et al.* (2006) as Chr4-*Adip11* is centered on a region also identified here as contributing to the epistatic architecture of fatpad weight.

The results of composite interval mapping also suggest that adjacent slQTL and epiQTL impact the mapping process. For example, there is a dramatic and unexpected increase in significance (nearly three orders of magnitude) for the additive slQTL peak at 134.82 Mb on chromosome 1 when composite interval mapping was applied (Figure 1A). While this is the most dramatic example, such effects were repeatedly observed (Figure S1) and on chromosomes 7 and 9, this resulted in the identification of two novel loci. Interestingly, this suggests that adjacent functional variants with opposite effects were fixed in the original parental lines during their production. Indeed, inspection of the regression coefficients from the full linear model shows that the epistatic peak closest to the slQTL signal at 134.82 Mb on chromosome 1 (DD with 12:73.42–89.12 Mb) and the marginal signal itself share a positive sign. However, the two slightly centromeric interactions involving the additive value on chromosome 1 (AA with 13:0–24.24 Mb and AD with 6:133.92–142.67 Mb) are both negative. Conditioning on these adjacent markers is indeed expected to enhance the signal of the neighboring additive effect, consistent with our observations. Thus, comparing the results of a conventional single-locus mapping model and composite interval mapping may be an indirect means of identifying neighboring functional variants. Further mapping in later generations of this advanced intercross will provide a great deal of additional information on the sign, magnitude, and physiological basis for these observed effects as recombination is expected to further separate their statistical signatures.

Conclusions: The application of multiple mapping approaches, including an epistatic model, is a vital strategy for characterizing complex genetic architectures. Contrary to suggestions based on human genome-wide association study findings, we found substantial numbers of pairwise epistatic interactions involving many more loci than show single-locus effects that account for an important portion of trait variation. This is likely due to the genetic structure of our experimental population where allele frequencies are intermediate; there are no rare alleles in our mapping system. This is critical since epistasis is known to produce predominantly additive and dominance variance when relatively rare alleles are involved (Cheverud and Routman 1995; Cheverud 2000).

Here, the use of a combination of techniques was further enhanced by the improved genetic resolution offered by AI lines. While single-locus scans remain the most tractable, pairwise epistatic relationships can now be dissected in great detail as well, and the identification of candidate loci for such interactions is possible. This is especially true for characters for which a large body of literature exists describing the mechanistic relationships among candidate genes and related pathologies. In such cases, incorporating *a priori* information regarding functional interactions can be used to help focus epistatic mapping studies and both ease the difficulties associated with multiple comparisons and facilitate the physiological interpretation of statistical results. It is an exciting prospect that even more fine-scale mapping of these loci will be possible in later generations of the LG,SM AI line. Undoubtedly future analyses, coupled with the incorporation of sequence information from the parental lines, will aid in further refining the physiological hypotheses presented here for fatpad variation and greatly contribute to our understanding of the statistical signatures of complex genetic architectures.

The authors acknowledge G. L. Fawcett and C. A. Lambert for offering insightful comments and suggestions on earlier drafts of this manuscript. This work was supported by a grant from the National Institutes of Health (DK-055736) and a doctoral dissertation improvement grant from the National Science Foundation (DEB-0608352).

LITERATURE CITED

Bartlett, M. S., and J. B. S. Haldane, 1935 The theory of inbreeding with forced heterozygosity. J. Genet. **31:** 327–340.

Bera, T. K., X-F. Liu, M. Yamada, O. Gavrilova, E. Mezey *et al.*, 2008 A model for obesity and gigantism due to disruption of the *Ankrd26* gene. Proc. Natl. Acad. Sci. USA **105**(1): 270–275.

Brachya, G., C. Yanay and M. Linial, 2006 Synaptic proteins as multi-sensor devises of neurotransmission. BMC Neurosci. **7**(Suppl 1): S4.

Brockmann, G. A., C. S. Haley, U. Renne, S. A. Knott and M. Schwerin, 1998 Quantitative trait loci affecting body weight and fatness from a mouse line selected for extreme high growth. Genetics **150:** 369–381.

Brockmann, G. A., J. Kratzsch, C. S. Haley, U. Renne, M. Schwerin *et al.*, 2000 Single QTL effects, epistasis, and pleiotropy account for two-thirds of the phenotypic F(2) variance of growth and obesity in DU6i x DBA/2 mice. Genome Res. **10**(12): 1941–1957.

Cao, Y., 2007 Angiogenesis modulates adipogenesis and obesity. J. Clin. Invest. **117**(9): 2362–2368.

Chai, C., 1956a Analysis of quantitative inheritance of body size in mice. I. Hybridization and maternal influence. Genetics **41:** 157–164.

Chai, C., 1956b Analysis of quantitative inheritance of body size in mice. II. Gene action and segregation. Genetics **41:** 165–178.

Chehab, F. F., 2008 Minireview: obesity and lipodystrophy—Where do the circles intersect? Endocrinology **149:** 925–934.

Cheverud, J. M., 2000 Detecting epistasis among quantitative trait loci, pp. 58–81 in *Epistasis and the Evolutionary Process*, edited by J. B. Wolf, E. D. Brodie and M. J. Wade. Oxford University Press, Oxford.

Cheverud, J. M., and E. J. Routman, 1995 Epistasis and its contribution to genetic variance components. Genetics **139:** 1455–1461.

Cheverud, J. M., E. J. Routman, F. A. M. Duarte, B. van Swinderen, K. Cothran *et al.*, 1996 Quantitative trait loci for murine growth. Genetics **142:** 1305–1319.

Cheverud, J. M., L. S. Pletscher, T. T. Vaughn and B. Marshall, 1999 Differential response to dietary fat in large (LG/J) and small (SM/J) inbred mouse strains. Physiol. Gen. **1:** 33–39.

Cheverud, J. M., T. T. Vaughn, L. S. Pletscher, A. C. Peripato, E. S. Adams *et al.*, 2001 Genetic architecture of adiposity in the cross of LG/J and SM/J inbred mice. Mamm. Genome **12:** 3–12.

Cheverud, J. M., T. H. Ehrich, J. P. Kenney, L. S. Pletscher and C. F. Semenkovich, 2004a Genetic evidence for discordance between obesity and diabetes-related traits in the LGXSM recombinant inbred mouse strains. Diabetes **53:** 2700–2708.

Cheverud, J. M., T. H. Ehrich, T. Hrbek, J. P. Kenney, L. S. Pletscher *et al.*, 2004b Quantitative trait loci for obesity and diabetes-related traits and their dietary responses to high fat feeding in the LGXSM recombinant inbred mouse strains. Diabetes **53:** 3328–3336.

Cheverud, J. M., G. L. Fawcett, J. P. Jarvis, E. A. Norgard, M. Pavlicev *et al.*, 2010 Calpain-10 is a component of the obesity-related quantitative trait locus *Adip1*. J. Lipid Res. **51:** 907–913.

Christians, J. K., A. Hoeflich and P. D. Keightley, 2006 *PAPPA2*, an enzyme that cleaves an insulin-like growth-factor-binding protein, is a candidate gene for a quantitative trait locus affecting body size in mice. Genetics **173:** 1547–1553.

Corva, P. M., S. Horvat and J. F. Medrano, 2001 Quantitative trait loci affecting growth in high growth (hg) mice. Mamm. Genome **12**(4): 284–290.

Darvasi, A., and M. Soller, 1995 Advanced intercross lines, an experimental population for fine genetic mapping. Genetics **141:** 1199–1207.

de Leeuw van Weenen, J. E., L. Hu, K. Jansen-Van Zelm, M. G. de Vries, J. T. Tamsma *et al.*, 2009 Four weeks high fat feeding induces insulin resistance without affecting dopamine release or gene expression patterns in the hypothalamus of C57Bl6 mice. Brain Res. **1250:** 141–148.

Doria, A., M. Patti and C. Kahn, 2008 The emerging genetic architecture of type 2 diabetes. Cell Metab. **8:** 186–200.

Duerr, R. H., K. D. Taylor, S. R. Brant, J. D. Rioux, M. S. Silverberg *et al.*, 2006 A genome-wide association study identifies IL23R as an inflammatory bowel disease gene. Science **314:** 1461–1463.

Elbatarny, H. S., S. J. Netherton, J. D. Ovens, A. V. Ferguson, and D. H. Maurice *et al.*, 2007 Adiponectin, ghrelin, and leptin differentially influence human platelet and human vascular endothelial cell functions: implication in obesity-associated cardiovascular diseases. Euro. J. Pharmacol. **558:** 7–13.

Fawcett, G. L., C. C. Roseman, J. P. Jarvis, B. Wang, J. B. Wolf *et al.*, 2008 Genetic architecture of adiposity and organ weight using combined generation QTL analysis. Obesity **16:** 1861–1868.

Fawcett, G. L., J. P. Jarvis, C. C. Roseman, B. Wang, J. B. Wolf *et al.*, 2010 Fine-mapping of obesity-related quantitative trait loci in an $F_{9/10}$ advanced intercross line. Obesity **18**(7): 1383–1392.

Fenske, T. S., C. McMahon, D. Edwin, J. C. Jarvis, J. M. Cheverud *et al.*, 2006 Identification of candidate alkylator-induced cancer susceptibility genes by whole genome scanning in mice. Cancer Res. **66:** 5029–5038.

Gabory, A., M-A. Ripoche, A. Le Digarcher, F. Watrin, A. Ziyyat *et al.*, 2009 *H19* acts as a trans regulator of the imprinted gene network controlling growth in mice. Development **136:** 3413–3421.

Gardner, M., J. Bertranpetit and D. Comas, 2008 Worldwide genetic variation in dopamine and serotonin pathway genes: Implications for association studies. Am. J. Med. Genet. B **147B**(7): 1070–1075.

Gat-Yablonski, G., and M. Phillip, 2008 Leptin and regulation of linear growth. Curr. Opin. Clin. Nutr. Metab. Care **11:** 303–308.

Haldane, J. B. S., and C. H. Waddington, 1931 Inbreeding and linkage. Genetics **16:** 357–374.

Haley, C. S., and S. A. Knott, 1992 A simple regression method for mapping quantitative trait loci in line crosses using flanking markers. Heredity **69:** 315–324.

Hanlon, P., W. A. Lorenz, Z. Shao, J. M. Harper, A. T. Galecki *et al.*, 2006 Three-locus and four-locus QTL interactions influence mouse insulin-like growth factor-I. Physiol. Genomics **26:** 46–54.

Hanson, W. D., 1959a The theoretical distribution of lengths of parental gene blocks in the gametes of an F_1 individual. Genetics **44:** 197–209.

Hanson, W. D., 1959b Theoretical distribution of the initial linkage block lengths intact in the gametes of a population intermated for n generations. Genetics **44:** 839–846.

Hanson, W. D., 1959c Early generation analysis of lengths of heterozygous chromosome segments around a locus held heterozygous with backcrossing or selfing. Genetics **44:** 833–837.

Hanson, W. D., 1959d The breakup of initial linkage blocks under selected mating systems. Genetics **44:** 857–868.

Hirai, S., M. Yamanaka, H. Kawachi, T. Matsui and H. Yano, 2005 Acitin A inhibits differentiation of 3T3–L1 preadipocyte. Mol. Cell. Endocrinol. **232:** 21–26.

Hoffmann, A-C., R. Mori, D. Vallbohmer, J. Brabender, E. Klein *et al.*, 2008 High expression of *HIF1a* is a predictor of clinical outcome in patients with pancreatic ductal adenocarcinomas and correlated to *PDGFA, VEGF,* and *bFGF.* Neoplasia **10**(7): 674–679.

Horvat, S., L. Bunger, V. M. Falconer, P. Mackay, A. Law *et al.*, 2000 Mapping of obesity QTLs in a cross between mouse lines divergently selected on fat content. Mamm. Genome **11**(1): 2–7.

Ichihara, S., and Y. Yamada, 2008 Genetic factors for human obesity. Cell. Mol. Life Sci. **65:** 1086–1098.

Ishimori, N., R. Li, P. M. Kelmenson, R. Korstanje, K. A. Walsh *et al.*, 2004 Quantitative trait loci that determine plasma lipids and obesity in C57BL/6J and 129S1/SvImJ inbred mice. J Lipid Res. **45**(9): 1624–1632.

Jannink, J.-L., M. C. A. M. Bink and R. C. Jansen, 2001 Using complex plant pedigrees to map valuable genes. Trends Plant Sci. **6:** 337–342.

Jarvis, J. P., and J. M. Cheverud, 2009 Epistatis and the evolutionary dynamics of measured genotypic values during simulated serial bottlenecks. J. Evol. Biol. **22:** 1658–1668.

Kahn, Z., S. Vijayakumar, T. Villanueva de la Torre, S. Rotolo and A. Bafico, 2007 Analysis of endogenous *LRP6* function reveals a novel feedback mechanism by which *Wnt* negatively regulates its receptor. Mol. Cell. Biol. **27:** 7291–7301.

Keightley, P. D., T. Hardge, L. May and G. Bulfield, 1996 A genetic map of quantitative trait loci for body weight in the mouse. Genetics **142:** 227–235.

Keightley, P. D., K. H. Morris, A. Ishikawa, V. M. Falconer and F. Oliver, 1998 Test of candidate gene–quantitative trait locus association applied to fatness in mice. Heredity **81**(Pt 6): 630–637.

Kenney-Hunt, J. P., B. Wang, E. A. Norgard, G. Fawcett, D. Falk *et al.*, 2008 Pleiotropic patterns of quantitative trait loci for 70 murine skeletal traits. Genetics **178:** 2275–2288.

Kim, J. H., S. Sen, C. S. Avery, E. Simpson, P. Chandler *et al.*, 2001 Genetic analysis of a new mouse model for non-insulin-dependent diabetes. Genomics **74**(3): 273–286.

Klein, R. J., C. Zeiss, E. Y. Chew, J-Y. Tsai, R. S. Sackler *et al.*, 2005 Complement Factor H Polymorphism in Age-Related Macular Degeneration. Science **308:** 385–389.

Kramer, M. G., T. T. Vaughn, L. S. Pletscher, K. King-Ellison, E. Adams *et al.*, 1998 Genetic variation in body weight growth and composition in the intercross of Large (LG/J) and Small (SM/J) inbred strains of mice. Genet. Mol. Biol. **21:** 211–218.

Lander, E. S., and D. Botstein, 1989 Mapping mendelian factors underlying quantitative traits using RFLP linkage maps. [published erratum appears in Genetics **136:** 705] Genetics **121:** 185–199.

Mani, A., J. Radhakrishnan, H. Wang, A. Mani, M-A Mani *et al.*, 2007 *LRP6* mutation in a family with early coronary disease and metabolic risk factors. Science **315**(5816): 1278–1282.

Mehrabian, M., P. Z. Wen, J. Fisler, R. C. Davis and A. J. Lusis, 1998 Genetic loci controling body fat, lipoprotein metabolism, and insulin levels in a multifactorial mouse model. J. Clin. Invest. **101**(11): 2485–2496.

Norgard, E. A., J. P. Jarvis, C. C. Roseman, T. J. Maxwell, J. P. Kenney-Hunt *et al.*, 2009 Replication of long bone length QTL in the F_9-F_{10} LG,SM advanced intercross. Mamm. Genome **20**: 224–235.

Papst, C., M. Bohn, H. F. Utz, A. E. Melchinger, D. Klein *et al.*, 2004 QTL mapping for European corn borer resistance (*Ostrinia nubilalis* Hb.), agronomic and forage quality traits of testcross progenies in early-maturing European maize (*Zea mays* L.) germplasm. Theor. Appl. Genet. **108:** 1545–1554.

Phillips, P. C., 2008 Epistasis-the essential role of gene interactions in the structure and evolution of genetic systems. Nat. Rev. Genet. **9**(11): 855–867.

R Development Core Team, 2009 *R: A Language and Environment for Statistical Computing.* R Foundation for Statistical Computing, Vienna. http://www.R-project.org.

Rockman, M. V., and L. Kruglyak, 2008 Breeding designs for recombinant inbred advanced intercross lines. Genetics **179:** 1069–1078.

Rosen, C. J., C. Ackert-Bicknell, W. G. Beamer, T. Nelson, M. Adamo *et al.*, 2005 Allelic differences in a quantitative trait locus affecting insulin-like growth factor-I impact skeletal acquisition and body composition. Pediatr. Nephrol. **20**(3): 255–260.

Silver, L. M., 1995 *Mouse Genetics: Concepts and Applications.* Oxford University Press, New York.

Sladek, R., G. Rocheleau, J. Rung, C. Dina, L. Shen *et al.*, 2007 A genome-wide association study identifies novel risk loci for type 2 diabetes. Nature **445:** 881–885.

Smith Richards, B. K., B. N. Belton, A. C. Poole, J. J. Mancuso, G. A. Churchill *et al.*, 2002 QTL analysis of self-selected macronutrient diet intake: fat, carbohydrate, and total kilocalories. Physiol. Genomics **11**(3): 205–217.

Sokal, R. S., and F. J. Rohlf, 1995 *Biometry.* W. H. Freeman, New York.

Stylianou, I. M., R. Korstanje, R. Li, S. Sheehan, B. Paigen *et al.*, 2006 Quantitative trait locus analysis for obesity reveals multiple networks of interacting loci. Mamm. Genome **17:** 22–36.

Taylor, B. A., and S. J. Phillips, 1996 Detection of obesity QTLs on mouse chromosomes 1 and 7 by selective DNA pooling. Genomics **34**(3): 389–398.

Taylor, B. A., C. Wnek, D. Schroeder and S. J. Phillips, 2001 Multiple obesity QTLs identified in an intercross between the NZO (New Zealand obese) and the SM (small) mouse strains. Mamm. Genome **12**(2): 95–103.

Togawa, K., M. Moritani, H. Yaguchi and M. Itakura, 2006 Multidimensional genome scans identify the combinations of genetic loci linked to diabetes-related phenotypes in mice. Hum. Mol. Genet. **15**(1): 113–128.

Tropea, A., F. Tiberi, F. Minici, M. Orlando, M. F. Gangale *et al.*, 2007 Ghrelin affects the release of luteolytic and luteotropic factors in human luteal cells. J. Clin. Endocrinol. Metab. **92**(8): 3239–3245.

Uchida, T., T. Nakamura, N. Hashimoto, T. Matsuda, K. Kotani *et al.*, 2005 Deletion of Cdkn1b ameliorates hyperglycemia by maintaining compensatory hyperinsulinemia in diabetic mice. Nat. Med. **11**(2): 175–182.

Vaughn, T. T., L. S. Pletscher, A. Peripato, K. King-Ellison, E. Adams *et al.*, 1999 Mapping quantitative trait loci for murine growth: a closer look at genetic architecture. Genet. Res. **74:** 313–322.

Warden, C. H., J. S. Fisler, S. M. Shoemaker, P. Z. Wen, K. L. Svenson *et al.*, 1995 Identification of four chromosomal loci determining obesity in a multifactorial mouse model. J. Clin. Invest. **95**(4): 1545–1552.

Wentzell, A. M., H. C. Rowe, B. G. Hansen, C. Ticconi, B. A. Halkier *et al.*, 2007 Linking Metabolic QTLs with Network and *cis*-eQTLs Controlling Biosynthetic Pathways. PLoS Genet. **3:** 1687–1701.

Werner, S., and C. Alzheimer, 2006 Roles of activin in tissue repair, fibrosis and inflammatory disease. Cytokine Growth Factor Rev. **17**(3): 157–171.

West, D. B., J. Goudey-Lefevre, B. York and G. E. Truett, 1994 Dietary obesity linked to genetic loci on chromosomes 9 and 15 in a polygenic mouse model. J. Clin. Invest. **94**(4): 1410–1416.

Wilson, R. H., T. J. Morgan and T. F. C. Mackay, 2006 High-resolution mapping of quantitative trait loci affecting increased life span in *Drosophila melanogaster.* Genetics **173:** 1455–1463.

Woodruff, T. K., and J. P. Mather, 1995 Inhibin, Activin and the female reproductive axis. Annu. Rev. Physiol. **57:** 219–244.

Yamauchi, T., Y. Nio, T. Maki, M. Kobayashi, T. Takazawa *et al.*, 2007 Targeted disruption of *AdipoR1* and *AdipoR2* causes abrogation of adiponectin binding and metabolic actions. Nat. Med. **13:** 332–339.

Yi, N., A. Diament, S. Chiu, K. Kim, D. B. Allison *et al.*, 2004 Characterization of epistasis influencing complex spontaneous obesity in the BSB model. Genetics **167**(1): 399–409.

Yi, N., D. K. Zinniel, K. Kim, E. J. Eisen, A. Bartolucci *et al.*, 2006 Bayesian analyses of multiple epistatic QTL models for body weight and body composition in mice. Genet. Res. **87**(1): 45–60.

Zeggini, E., L. J. Scott, R. Saxena, B. F. Voight, J. L. Marchini *et al.*, 2008 Meta-analysis of genome-wide association data and large-scale replication identifies additional susceptibility loci for type 2 diabetes. Nat. Genet. **40**(5): 638–645.

Zeng, Z. B., 1994 Precision mapping of quantitative trait loci. Genetics **136:** 1457–1468.

Ziemke, F., and C. S. Mantzoros, 2010 Adiponectin in insulin resistance: lessons from translational research. Am. J. Clin. Nutr. **91**(Suppl): 258S–261S.

Communicating editor: L. M. McIntyre

GENETICS

Supporting Information
http://www.genetics.org/cgi/content/full/genetics.110.123505/DC1

Mapping the Epistatic Network Underlying Murine Reproductive Fatpad Variation

Joseph P. Jarvis and James M. Cheverud

Copyright © 2011 by the Genetics Society of America
DOI: 10.1534/genetics.110.123505

File S1

Supporting Data

File S1 is available for download as a .csv file at http://www.genetics.org/cgi/content/full/genetics.110.123505/DC1.

Animal, Sire, and Dam IDs are given for all individuals used in these analyses along with sex, age at necropsy (in days), whether they were used as breeders for the F_{11} generation, their reproductive fatpad weight (in grams) and all measured genotypes given as -1, 0 and 1 indicating SS, LS/SL and LL genotypes respectively.

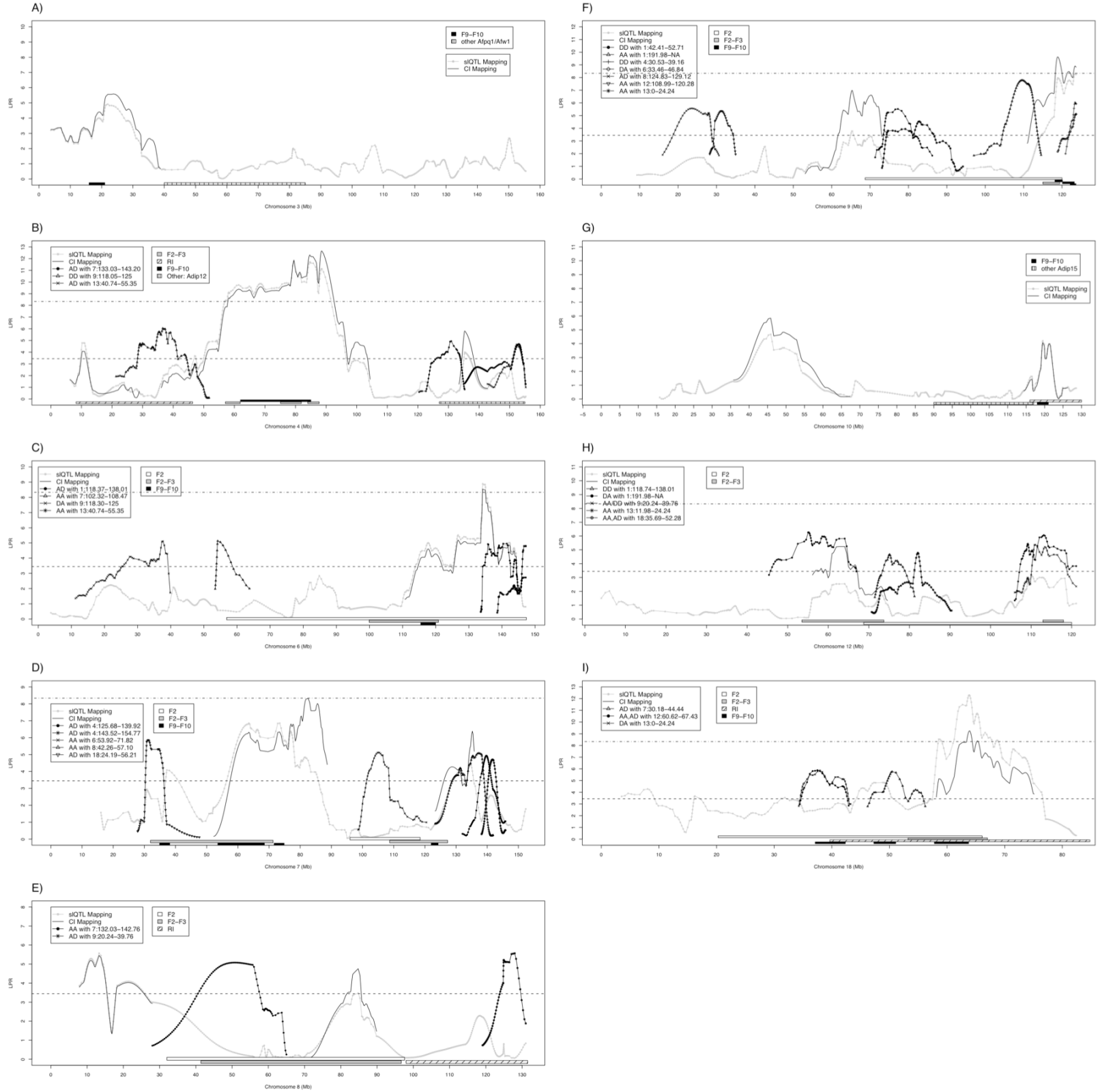

FIGURE S1.—Mapping results for the remaining chromosomes that harbor slQTL for reproductive fatpad weight in the F_{10} of the AIL 3 (A), 4 (B), 6 (C), 7 (D), 8 (E), 9 (F), 10 (G), 12 (H) and 18 (I). Results from the single-locus model are given as connected grey dots, composite interval mapping as smooth black lines and epistatic interactions by other connected shapes. Confidence intervals from previous analyses are represented by horizontal bars below each QTL plot.

FIGURES S2-S20

Figures S2-S20 are available for download as individual PDF files at http://www.genetics.org/cgi/content/full/genetics.110.123505/DC1.

FIGURE S2-20.—Heat maps graphically depicting the mapping results from the genome-wide scan for epistasis. Each figure has consistent x-axes representing a given chromosome, y-axes represent the second chromosome in the mapping model and color represents LPR score for the particular test. Colors change at breakpoints of LPR = 3.44 (the minimum threshold value, see text), 4, 5, 6, 7, 8, 9, 10, 11, 12, 13, 14, 15 , 16, 17, 18, and 19 with the associated colors: "violet", "lightblue", "royalblue", "lightgreen", "forestgreen", "yellowgreen", "yellow", "goldenrod", "orange", "darkorange", "lightpink", "red", "darkred", "black", "grey", and "white". Thus, lightblue indicates an epistatic LPR score greater than 4 but less than 5.

TABLE S1

The 199 slQTL and epiQTL peaks that cluster into roughly 73 separate confidence intervals that show significant marginal and/or epistatic effects in chromosome specific models. Terms included in the slQTL system (see text) are given in bold.

Table S1 is available for download as an Excel file at http://www.genetics.org/cgi/content/full/genetics.110.123505/DC1.